JOURNAL OF MATERIALS SCIENCE: MATERIALS IN MEDICINE **16** (2005) 647–654

Control of surface morphology of carbide coating on Co-Cr-Mo implant alloy

N. S. VANDAMME, L. D. T. TOPOLESKI*
Department of Mechanical Engineering, UMBC, Baltimore, MD 21250, USA
E-mail: topoleski@umbc.edu

Wear of materials used in artificial joints is a common failure mode of artificial joints. A low wear rate for implants is believed to be critical for extending implant service time. We developed a carbide-coated Co-Cr-Mo implant alloy created in plasma of methane and hydrogen mixed gas by a microwave plasma-assisted surface reaction. The carbide-coated Co-Cr-Mo has a unique "brain coral-like" surface morphology and is much harder than uncoated Co-Cr-Mo. The effect of plasma processing time and temperature on the surface morphology of the top carbide layer was studied toward optimizing the surface coating. The ratios of average roughness, R_a, core roughness, R_k, and summation of core roughness, reduced peak height (R_{pk}) and reduced valley depth (R_{vk}), $R_k + R_{pk} + R_{vk}$, for the 6-h/985 °C coating to those for the 0.5-h/985 °C coating were 1.9, 1.7, and 1.9, respectively. The ratios of R_a, R_k, and $R_k + R_{pk} + R_{vk}$ for the 4-h/1000 °C coating to those for the 4-h/939 °C coating were 2.3, 2.3, and 2.0, respectively. With the proper combination of plasma processing time and temperature, it may be possible to change the thickness of the peak-valley top cluster by fourfold from ~0.6 μm to ~2.5 μm. Finally, the growth mechanism of the carbide layers on Co-Cr-Mo was discussed in the context of atomic composition analysis.

1. Introduction

The biomedical applications of cobalt-chromium-base alloys started in 1932 in dentistry and were expanded to orthopedic prostheses in the 1950s [1]. Cobalt-base alloys are also known to be some of the superalloys whose development for elevated-temperature applications started in the 1930s [2]. Since then, Co-base alloy technology has improved continuously and Co-base alloys are now playing important roles in many applications.

The Co-Cr-Mo alloy is one of the most used implant alloys for artificial joints and provides a good combination of mechanical properties, corrosion resistance, and biocompatibility [3]. Improving artificial joints to increase their service life has been urged by arthritis patients of all ages to enhance their improved and more active lifestyles.

Wear of materials used in artificial joints is a common failure mode of artificial joints. A low wear rate for implants is believed to be critical for extending implant service time. The current revival of metal-on-metal articulating couples was motivated by the problem of excessive amounts of polyethylene wear debris, which has been linked to osteolysis and subsequent implant loosening [4, 5]. Ceramics have been investigated as excellent wear resistant materials in combination with ultra-high molecular weight polyethylene, alloys, and ceramics [6–8]. Surface modifications such as diamond-like carbon coating or ion implantation are other important approaches to improving wear resistance [9, 10].

In the course of our project on the surface modification of Co-Cr-Mo implant alloy to increase its wear resistance, we developed a carbide-coated Co-Cr-Mo created by a microwave plasma-assisted surface reaction between the alloy surface and a mixed gas of methane and hydrogen [11]. The carbide-coated Co-Cr-Mo has a unique "brain coral-like" surface morphology and a range of hardness from HV 1000 to HV 2100, which is much greater than the uncoated Co-Cr-Mo (HV 430). Although the carburization of superalloys in an aggressive environment is one of the corrosion phenomena leading to a structural degradation in some applications [12, 13], the "brain coral-like" surface morphology may have the advantages of retaining lubricant between the contacting solid interfaces and trapping debris which cause third-body abrasion in artificial joint applications.

In our previous paper we reported wear tests carried out using a sapphire ball on Co-Cr-Mo disc unidirectional configuration under harsh wear conditions [14]. The wear factor of carbide coated Co-Cr-Mo discs was slightly smaller than that of uncoated Co-Cr-Mo discs with deionized water lubrication. Optimizing the carbide surface morphology and proper selection of the

*Author to whom all correspondence should be addressed.

bearing material combination are important to effectively apply the high hardness and characteristic morphology of the carbide coated Co-Cr-Mo for use in artificial joints as a wear resistant material.

This paper reports on the effect of plasma processing time and temperature on surface characteristics of carbide coated Co-Cr-Mo implant alloy. This study is an initial step toward the long-term goal to obtain an optimized surface for an artificial joint.

2. Materials and methods

A wrought Co-Cr-Mo alloy rod (ASTM F1537, Teledyne Allvac) of 0.625 inch in diameter was cut into 7-mm thick discs. The primary composition of the alloy given by the manufacturer's specifications was (in wt%): 64.85 Co, 27.66 Cr, 5.70 Mo, 0.64 Mn, 0.64 Si, 0.23 Ni, 0.19 Fe and 0.048 C. Prior to plasma processing, the top and bottom flat planes of the discs were polished to a "mirror finish" with #600 and #1000 SiC abrasive paper, then with a 3-μm diamond suspension, and ultrasonically cleaned with acetone. The cylindrical side surface and rounded edges were also similarly polished but had a rougher finish. The average roughness of the mirror finish surface was $\sim$0.01 μm, measured with a white light interference surface profilometer (WLISP) (NewView 100, Zygo Corp., CT).

The microwave plasma-assisted reaction was carried out using our microwave plasma-assisted chemical vapor deposition system equipped with a tubular fused quartz reaction chamber with a 34 mm inner diameter. The microwave generator (Toshiba Corp., Tokyo) provides a range of microwave power from 0.1 to 1.5 kW at a frequency of 2.45 GHz. The Co-Cr-Mo specimens were mounted on a tantalum wire basket holder and inserted into a confined plasma space on a fused quartz rod. Plasma processing was carried out in a mixture of methane (ultra high purity 99.97%) and hydrogen (zerograde 99.99%) with a total gas pressure of 70 Torr and a total gas glow rate of 100 sccm (1 sccm of methane and 99 sccm of hydrogen). Before introducing methane, the specimens were pretreated in hydrogen plasma for 20 min. The specimen temperature was controlled by changing the microwave input power and measured with an optical pyrometer (Leeds and Northrup Model 8622) and an infrared thermometer (M90H, Mikron Instrument Co., NJ) through the quartz-glass viewport at the top of the reaction chamber. The emissivity value for Co-Cr-Mo of 0.27 was set on the infrared thermometer during the carbide formation reaction.

The weight change of discs caused by the reaction was measured using an analytic balance (AX205, Mettler-Toledo, Inc., OH) with a scale interval of 0.01 mg.

The surface morphology of carbide coated Co-Cr-Mo discs was studied using the WLISP. The roughness parameters, including average roughness, R_a, core roughness, R_k, reduced peak height, R_{pk}, reduced valley depth, R_{vk}, number of peaks or valleys, and distance between peaks or valleys (peak spacing or valley spacing), were averaged from measurements taken at seven equally spaced locations along the diameter of each disc. The filter cutoff wavelength, which differentiates between roughness and waviness, was fixed at 20 μm after measuring the cutoff wavelength dependence of the average roughness and core roughness of three carbide-coated specimens. The surface morphology was also observed and documented with a scanning electron microscope (SEM) (JEOL JSM-35CF).

Electron-probe X-ray quantitative analysis and dot mapping were carried out with an energy-dispersive spectrometer (JEOL JSM-5600). Preliminary results of surface chemical analysis were obtained by X-ray photoelectron spectroscopy (XPS) analysis using an SSI SSX-100 with Al K_α monochrometer and small spot size capability.

3. Results and discussion

3.1. Plasma processing time dependence

One disk was plasma-processed at 985 $\pm$ 10 °C for each of the following time periods: 0.5, 1.0, 2.0, 4.0, and 6.0 hs for a total of five disks. Silver colored metal carbide was formed on the whole surface of all specimens by the reaction between carbon atoms decomposed from methane and alloy surface metals. The coating morphology of the bottom of the discs was slightly different from that of the top plane. The bottom plane of discs, which made contact with tantalum wire of the basket holder on the fused quartz rod, had a few tiny golden colored spots and a small circular pattern in the center. Therefore only the top plane was used for surface morphology studies.

The weight gain divided by the whole surface area of the Co-Cr-Mo discs increased with an increase in plasma processing time shown in Fig. 1, where the coating was assumed to be uniform over the whole disc area. This growth curve followed the parabolic equation,

$$\Delta W = (7.0\, t)^{1/2} \tag{1}$$

where ΔW is weight gain per unit area in mg/cm^2 and t is processing time in hours. The parabolic relationship between ΔW and t is commonly observed in conventional steel carburization, where the kinetics of the carburization reaction are controlled by carbon diffusion processes [12, 13, 15, 16]. It was also reported that

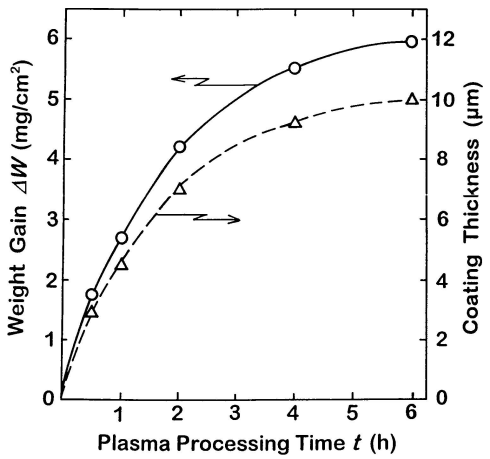

Figure 1 Weight gain in Co-Cr-Mo alloy discs and carbide coating thickness as a function of plasma processing time at plasma processing temperature of 985 °C.

the relationship between the carburized layer depth and carburizing time followed a parabolic rate law in DC plasma carburization of steel [17, 18].

The coating thickness plotted in Fig. 1 was calculated from the weight gain, total surface area, and the apparent density of the coating (6.0 g/cm^3). The apparent density value was estimated from the coating thickness determined from SEM micrographs of a polished section of the side plane of the substrate and the weight gain [11]. Our metal carbide coatings consist of mixed phases including Cr_3C_2-type, Cr_7C_3-type, and $Cr_{23}C_6$-type carbides and a porous structure [11]. The crystalline densities calculated from the unit cell dimensions of Cr_3C_2, Cr_7C_3, and $Cr_{23}C_6$ are 6.64, 6.91, and 6.96 g/cm^3, respectively [19].

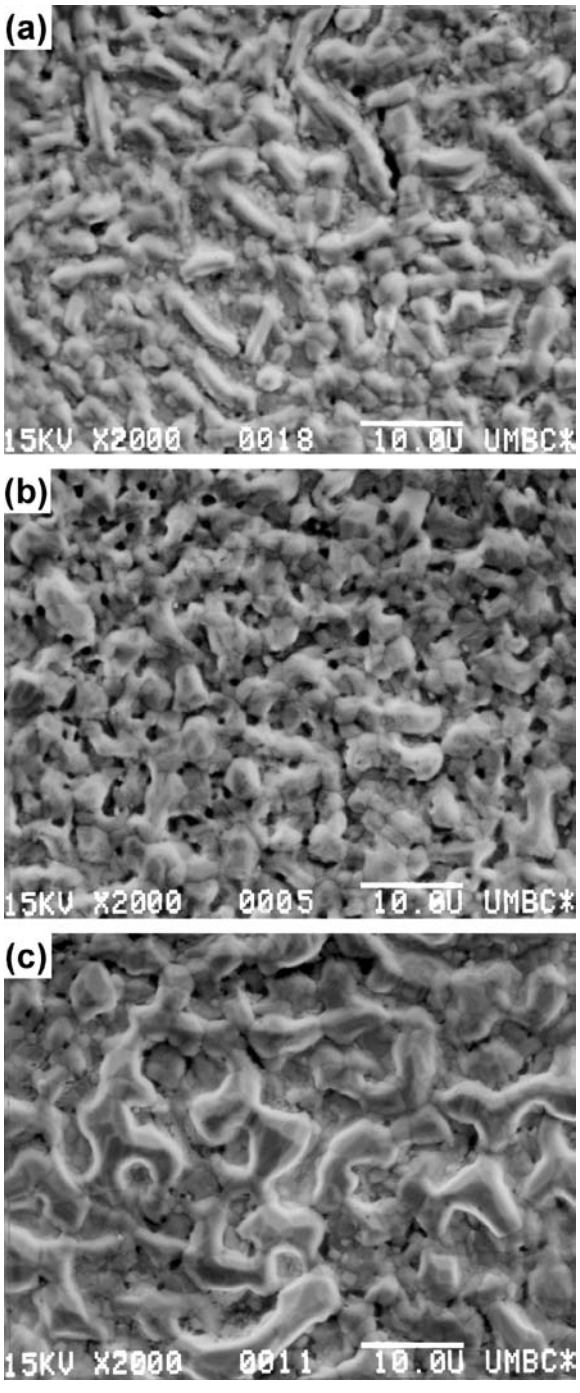

Figure 2 Scanning electron micrographs of carbide coated Co-Cr-Mo discs with plasma processing time of (a) 0.5 h, (b) 2.0 h, and (c) 4.0 h.

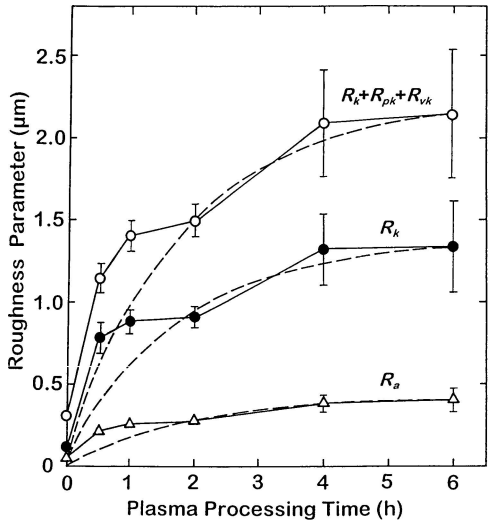

Figure 3 Roughness parameters, R_a, R_k, and $R_k+R_{pk}+R_{vk}$, vs. plasma processing time. Three dashed lines near each set of data points are the hypothetical growth curve whose end points are zero and 6-h values using the parabolic growth equation. The vertical bar on each data point represents the standard deviation for averaged values of seven measurements, as in Fig. 4, 8, and 9.

Micrographs of carbide coatings with 0.5-, 2.0-, and 4.0-h processing times show processing time dependence on surface morphology (Fig. 2). Since the micrographs do not represent a sequential analysis using an identical specimen, the growth process of individual crystal grains can not be traced, but the grains of the top layer appear to widen with processing time.

Average roughness, R_a, core roughness, R_k, summation of core roughness, reduced peak height (R_{pk}) and reduced valley depth (R_{vk}), $R_k+R_{pk}+R_{vk}$, the number of peaks or valleys in the area of 85 μm $\times$ 64 μm, and the distance between peaks or valleys (peak spacing or valley spacing) were selected from over thirty surface roughness parameters available from our profilometry applications to effectively quantify the surface characteristics of the present carbide coatings.

R_a, R_k, and $R_k + R_{pk} + R_{vk}$ increased with plasma processing time and leveled off after approximately 4 h (Fig. 3). The data point at 0-h was taken on a specimen after 20-min. hydrogen plasma pretreatment at 985 $\pm$ 10 °C, which clarified the grain boundaries on the Co-Cr-Mo disc by thermal etching. Three dashed lines near each set of data points are the hypothetical growth curves whose end points are zero and 6-h values (based on Equation (1)). Data points for less than 2 h deviated upward from the hypothetical growth curve. The ratios of R_a, R_k, and $R_k + R_{pk} + R_{vk}$ at 6 h to these roughness parameters at 0.5 h were 1.9, 1.7, and 1.9, respectively (Table I). It should be noted that a

TABLE I Ratios of surface roughness parameters of carbide top layer with different processing time and temperature

Parameters	6 h/0.5 h	1000 °C/939 °C
R_a	1.9	2.3
R_k	1.7	2.3
$R_k + R_{pk} + R_{vk}$	1.9	2.0
Average of peak spacing and valley spacing	1.2	1.1

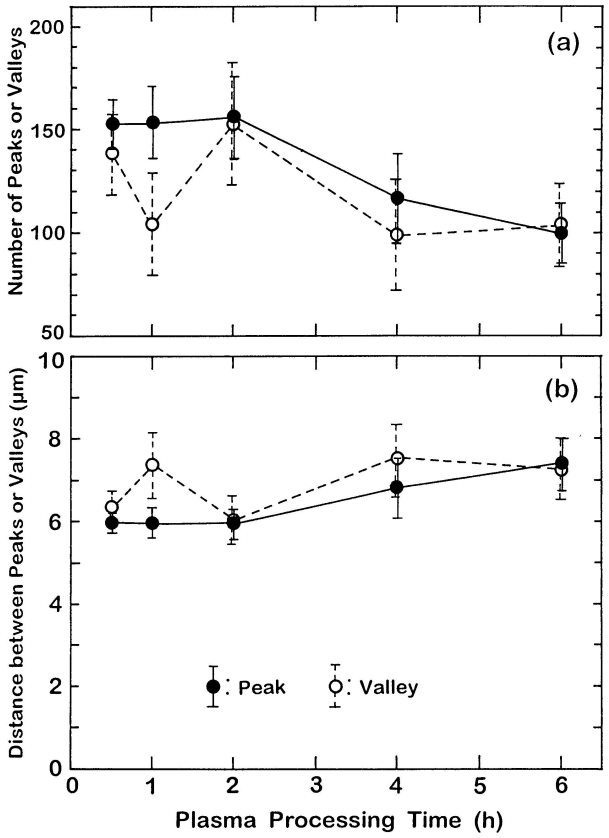

Figure 4 (a) Number of peaks or valleys in the area of 85 μm × 64 μm vs. plasma processing time and (b) distance between peaks or valleys (peak spacing or valley spacing) vs. plasma processing time.

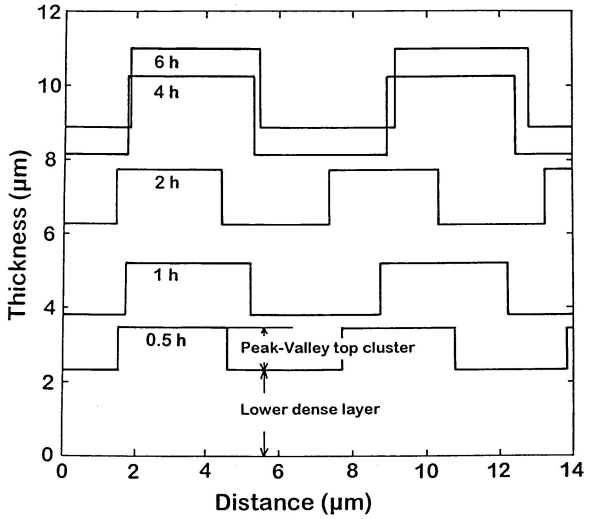

Figure 5 Simplified model of plasma processing time dependence of cross-sectional profile of carbide coatings at plasma processing temperature of 985 °C.

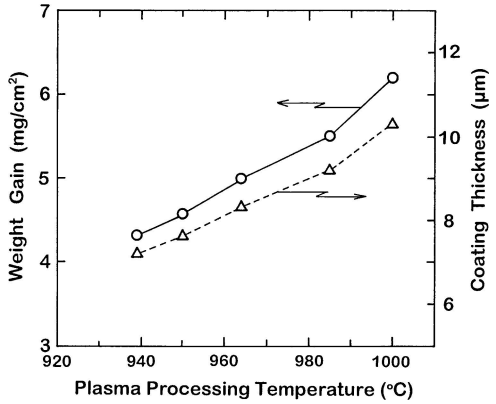

Figure 6 Weight gain in Co-Cr-Mo alloy discs and carbide coating thickness as a function of plasma processing temperature for 4-h plasma processing time.

considerably rough surface structure has already been produced at an early stage of carbide formation at 0.5 h. The number of peaks or valleys, and the distance between peaks or valleys (peak spacing or valley spacing) changed slightly with plasma processing time (Fig. 4). The ratio of average of peak spacing and valley spacing at 6 h to the average spacing at 0.5 h was 1.2 (Table I). The total peak area was equal to the total valley area within ±8% at all measurements.

Using the values of $R_k + R_{pk} + R_{vk}$, average of peak spacing and valley spacing, and thickness of the lower dense layer which was calculated by subtracting $(R_k + R_{pk} + R_{vk})/2$ from the coating thickness plotted in Fig. 1, the plasma processing time dependence of the cross-sectional profile of carbide coatings is illustrated using a simplified model (Fig. 5). While the thickness of the lower dense layer for 6.0-h carbide was 4 times that for 0.5-h carbide, the thickness of the peak-valley top cluster for 6.0-h carbide was 2 times that for 0.5-h carbide. The width of peaks or valleys for 6.0-h carbide was 1.2 times that for 0.5-h carbide. It should be noted that the skeleton of the top surface morphology was established at an early stage of carbide formation and preserved afterward without drastic changes or coalescence of neighboring crystalline grains.

3.2. Plasma processing temperature dependence

One disk was plasma-processed for four hours at each of the following plasma processing temperature: 939, 950, 964, 985, and 1000 °C (±5 °C) for a total of five disks. Silver colored metal carbide was formed over the entire surface of all specimens. After the run at 939 °C, a small amount of black soot-like deposit was found on the tantalum wire basket holder. This temperature may be the lower limit to produce metal carbide layers on Co-Cr-Mo free of diamond film, soot, or diamond particles under the present conditions [11, 14]. Again, only the top plane of the discs was used for surface morphology studies.

The weight gain per unit area and coating thickness increased with an increase in plasma processing temperature (Fig. 6). The activation energy can be calculated from an Arrhenius plot using the following equations [13],

$$(\Delta W)^2 = Kt \tag{2}$$

$$K = C \exp(-\Delta E/RT) \tag{3}$$

where ΔW is weight gain per unit area, K is a reaction rate constant, t is plasma processing time, C is a constant, ΔE is the activation energy, R is the Gas constant 8.314 J mol^{-1} K^{-1}, and T is plasma processing temperature. The activation energy of metal carbide layer

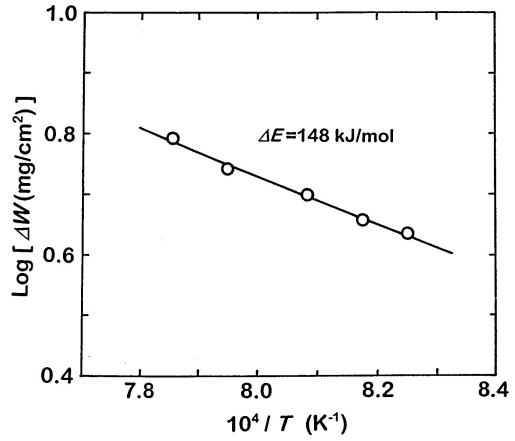

Figure 7 Arrhenius plot of temperature dependence of carbide growth on Co-Cr-Mo implant alloy by a microwave plasma-assisted reaction.

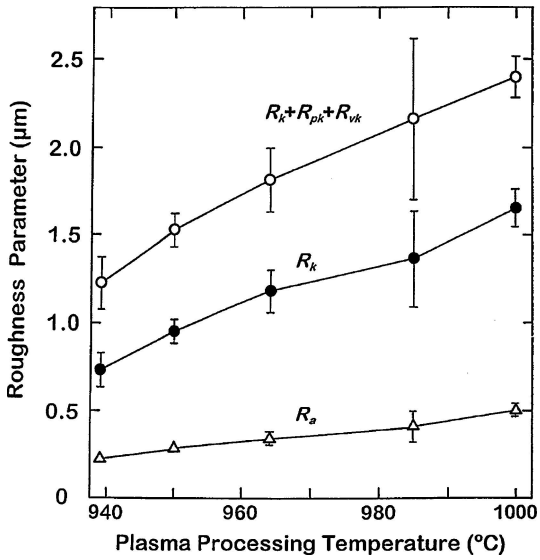

Figure 8 Roughness parameters, R_a, R_k, and $R_k + R_{pk} + R_{vk}$, vs. plasma processing temperature.

formation on Co-Cr-Mo alloy by a microwave plasma-assisted reaction was obtained to be 148 kJ/mol (Fig. 7). No data on the activation energy for the carburization of Co-Cr-Mo alloy exists to our knowledge. This value is closer to the activation energy for the carburization of iron-based alloys such as alloy 310 stainless steel (130 kJ/mol) or alloy 556 (170 kJ/mol) than that for Ni-Cr alloy 214 (235 kJ/mol) or ternary carbide Ti_3SiC_2 (351 kJ/mol) [13, 20].

R_a, R_k, and $R_k + R_{pk} + R_{vk}$ increased monotonically with an increase in plasma processing temperature (Fig. 8). The ratios of R_a, R_k, and $R_k + R_{pk} + R_{vk}$ at 1000 °C to these roughness parameters at 939 °C are 2.3, 2.3, and 2.0, respectively (Table I). The number of peaks or valleys changed slightly, generally decreasing with an increase in temperature, and accordingly the distance between peaks or valleys (peak spacing or valley spacing) changed slightly, generally increasing with an increase in temperature (Fig. 9). The ratios of peak spacing, valley spacing, and average of peak spacing and valley spacing at 1000 °C to these spacings at 939 °C are 1.1, 1.2, and 1.1, respectively (Table I). The total peak area was equal to the total valley area within ±5% at all temperatures.

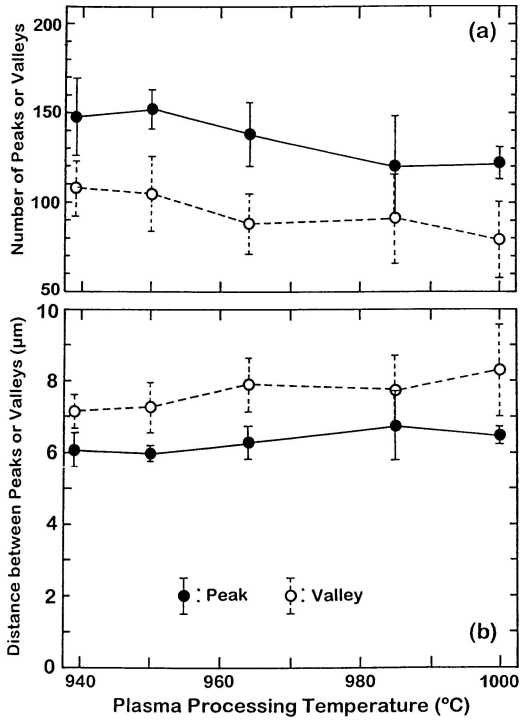

Figure 9 (a) Number of peaks or valleys in the area of 85 μm × 64 μm vs. plasma processing temperature and (b) distance between peaks or valleys (peak spacing or valley spacing) vs. plasma processing temperature.

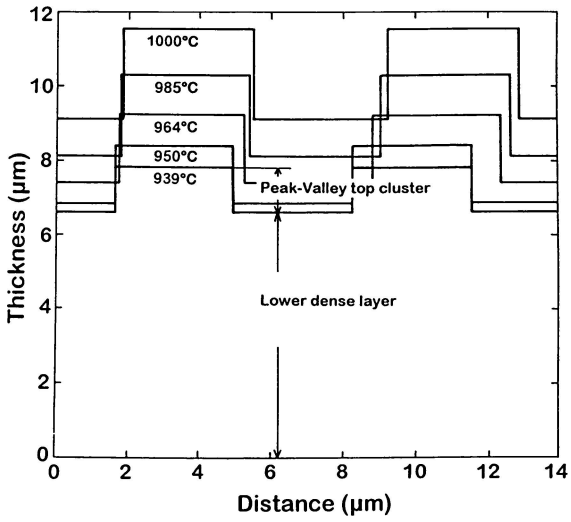

Figure 10 Simplified model of plasma processing temperature dependence of cross-sectional profile of carbide coatings for 4-h plasma processing time.

The plasma processing temperature dependence of the cross-sectional profile of carbide coatings is illustrated using a simplified model (Fig. 10). While the thickness of the lower dense layer for 1000 °C-carbide was 1.4 times that for 939 °C-carbide, the thickness of the peak-valley top cluster for 1000 °C-carbide was 2 times that for 939 °-carbide. The width of peaks or valleys for 1000 °C-carbide was 1.1 times that for 939 °-carbide. The thickness of the peak-valley top cluster was more sensitive to the plasma processing temperature than the thickness of the lower dense layer and the width of peaks or valleys.

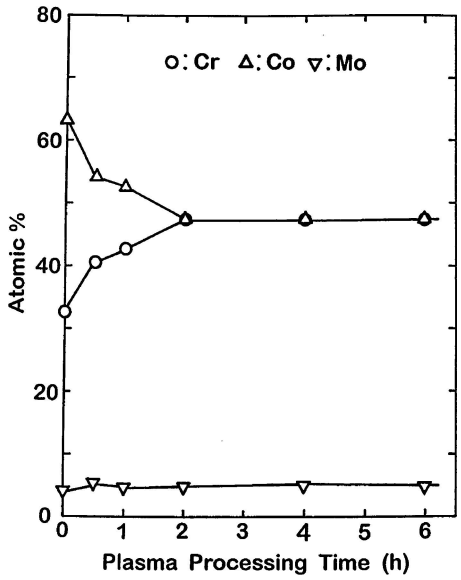

Figure 11 Electron-probe X-ray quantitative analysis of carbide coated Co-Cr-Mo vs. plasma processing time at plasma processing temperature of 985 °C.

With the proper combination of plasma processing time and temperature from the ranges used in this study, it may be possible to change the thickness of the peak-valley top cluster by up to fourfold, from ~0.6 to ~2.5 μm, the width of peaks or valleys by 30% around 3–4 μm, and the thickness of the lower dense layer by up to six-fold, from ~1.5 to ~9.7 μm.

3.3. Growth mechanism of brain coral-like carbide layers on Co-Cr-Mo implant alloy

The effect of plasma processing time on the atomic concentration of Co, Cr, and Mo in the surface layer was studied by X-ray quantitative analysis (Fig. 11). The surface of uncoated Co-Cr-Mo consisted of 63.5-at% Co, 33.0-at% Cr, and 5.0-at% Mo. The concentration of Co decreased and that of Cr increased with an increase in plasma processing time, until 2 h. The surface of carbide coated Co-Cr-Mo with a plasma processing time longer than 2 h contained an equal atomic concentration of Co and Cr. The concentration of Mo was almost constant at 5.0 at% in all samples. When the carbide layer is thin, signals not only from the carbide layer but also signals from the Co-Cr-Mo substrate under the carbide layer contribute to the measured concentration. The time dependence of atomic concentration in the early stage may not represent solely the composition of the carbide layer. In the case of the thick carbide layer, the atomic concentration is likely for the carbide layer only.

Preliminary results by XPS were obtained on 6-h carbide coated Co-Cr-Mo [21]. The peak which might have three or four components at 574.5–578.3 eV could be assigned to chromium carbide. After ~100 nm etching of the surface layer with Ar^+ ions, the atomic concentration ratio of C:Cr:Co was 1:1:1.

X-ray elemental dot mapping results (Fig. 12) show the effect of plasma processing time on the spatial

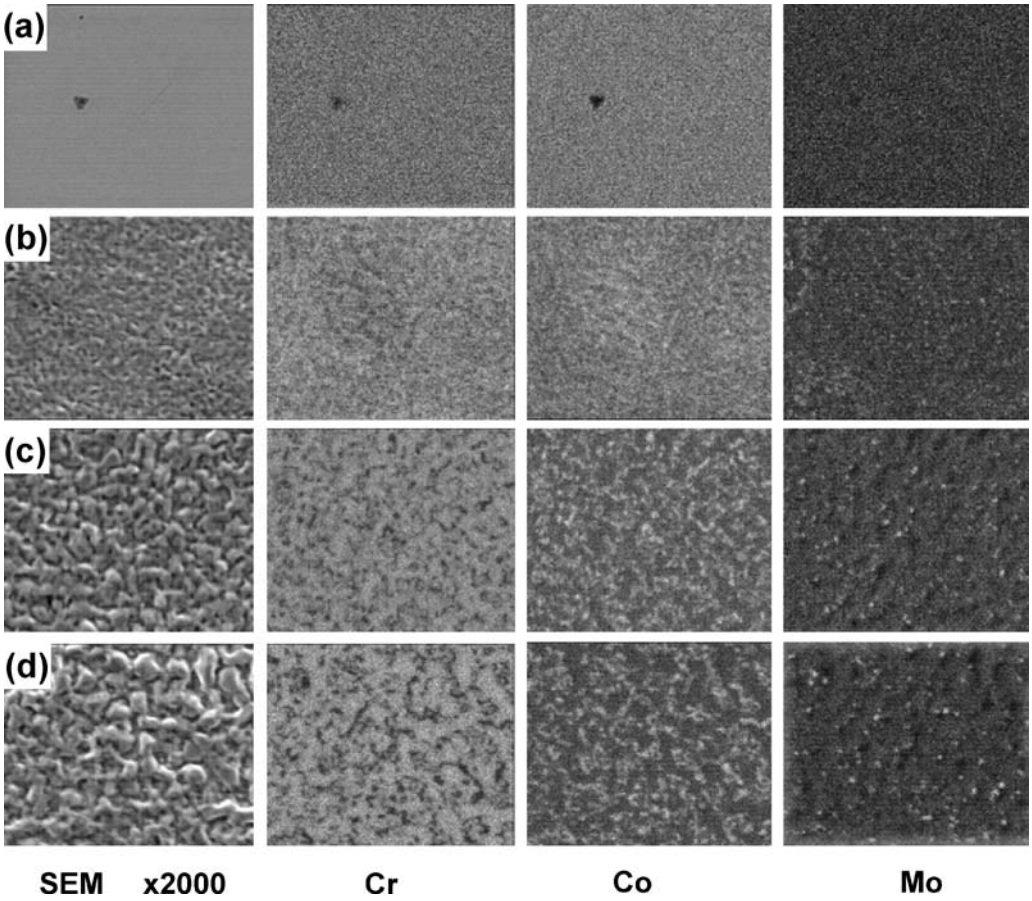

Figure 12 X-ray dot mapping of (a) uncoated Co-Cr-Mo disc and carbide coated Co-Cr-Mo discs with plasma processing time of (b) 0.5 h, (c) 2.0 h, and (d) 6.0 h at plasma processing temperature of 985 °C.

location, which was indicated by fine white dots, of component elements. While Cr, Co, and Mo atoms were uniformly distributed on the uncoated Co-Cr-Mo, Cr atoms were localized in the peak areas and Co atoms were localized in the valley areas of the carbide top cluster. The localized and distinctively isolated spots of Mo atoms were observed on carbide coated Co-Cr-Mo, but their relation to the morphology is not clear. The elemental dot mapping is only qualitative, conveying the spatial location of constituents, but not the amount present [22].

It appears that Cr atoms selectively react with atomic or ionic carbons and produce Cr carbide compounds on the surface of Co-Cr-Mo alloy exposed to reaction gases in microwave plasma. The crystalline nuclei of Cr carbides may grow as isolated island crystals and then connect together, with an increase in plasma processing time, to form the remarkable "brain coral-like" morphology. Stable compounds of Cr carbides are Cr_3C_2, Cr_7Cr_3, and $Cr_{23}C_6$, but Co can be mixed into Cr sites of Cr_7C_3 up to 26wt% and into Cr sites of $Cr_{23}C_6$ up to 20 wt% [23].

Since the geometry of the peak-valley top cluster did not change drastically with changing plasma processing time and temperature, two models were considered. Model 1 is that new layers are formed and accumulated in both peak and valley areas while preserving the skeleton of morphology during the growing process. Model 2 is that crystalline grains which create peaks are preserved in their almost original geometry and composition and the formation of a new carbide layer proceeds mainly in the lower dense layer, namely in valley areas and under the bottom of peak areas. It can not be concluded at present which model is predominant. More studies may be needed to elucidate the growth mechanism.

4. Conclusions

A motivation for this study was that the carbide coated Co-Cr-Mo implant alloy with a brain coral-like morphology showed potential as a wear resistant material for artificial joint applications in our previous wear test study. There, only one kind of carbide coated Co-Cr-Mo disc was produced with one set of plasma processing variables. Here two variables, plasma processing time and temperature, were examined to see whether the surface morphology could be controlled. We found that it might be possible to change the thickness of the peak-valley top cluster, which is a feature of brain coral-like morphology, by fourfold: from ~0.6 to ~2.5 μm, and the width of peaks or valleys by 30%: around 3–4 μm, with the proper combination of plasma processing time and temperature. If the growth mechanism and the microstructure of the interface between Co-Cr-Mo substrate and carbide layer can be elucidated, the control of the morphology will be more refined. If other factors, such as surface pretreatment of the substrate, play a role, different morphologies may be obtained. The metal components of currently used artificial joints have extremely smooth surfaces (typically around 0.01μm R_a), and it is tempting to conclude that the contacting area of the brain coral-like surface must be similarly smooth. However, we do not know the tribological properties of the brain coral-like surfaces, specifically the optimum surface morphology for retaining lubricant and trapping/removing wear debris. The next stage of this research is to conduct wear experiments to test carbide coated Co-Cr-Mo discs with different surface structures—varying from the original surface morphology to a polished, smooth carbide layer—against counterbodies such as uncoated Co-Cr-Mo, carbide coated Co-Cr-Mo, or polyethylene.

Acknowledgments

The authors would like to thank Mr. E. Moore of the Physics Department of UMBC for X-ray quantitative analysis and elemental dot mapping and Dr. C. R. Anderson of Anderson Materials Evaluation, Inc. for XPS measurements. This work was partially supported by a grant from the Arthritis Foundation.

References

1. BATTELLE MEMORIAL INSTITUTE, "Cobalt Monograph" edited by Centre d'Information du Cobalt (M. Weissenbruch LTD., Belgium, 1960) pp. 416 and 509.
2. C. T. SIMS, in "The Superalloys" edited by C. T. Sims and W. C. Hagel (John Wiley & Sons, New York, 1972) p. 145.
3. J. A. DISEGI, R. L. KENNEDY and R. PILLIAR, in "Cobalt-Base Alloys for Biomedical Appliations," edited by J. A. Disegi, R. L. Kennedy and R. Pilliar (American Society for Testing and Materials, West Conshohocken, PA, 1999).
4. H.-G. WILLERT, H. BERTRAM and G. H. BUCHHORN, *Clin. Orthop. Relat. Res.* **258** (1990) 95.
5. H. C. AMSTUTZ, P. CAMPBELL, N. KOSSOVSKY and I. C. CLARKE, *ibid.* **276** (1992) 7.
6. D. DOWSON, *Wear* **190** (1995) 171.
7. J. E. NEVELOS, E. INGHAM, C. DOYLE, A. B. NEVELOS and J. FISHER, *Biomaterials* **22** (2001) 2191.
8. K. TANAKA, J. TAMURA, K. KAWANABE, M. NAWA, M. OKA, M. UCHIDA, T. KOKUBO and T. NAKAMURA, *J. Biomed. Mater. Res.* **63** (2002) 262.
9. P. FIRKINS, J. L. HAILEY and J. FISHER, *J. Mat. Sci.: Mater. in Med.* **9** (1998) 597.
10. H. A. MCKELLOP and T. V. RÖSTLUND, *J. Biomed. Mater. Res.* **24** (1990) 1413.
11. N. S. VANDAMME, L. QUE and L. D. T. TOPOLESKI, *J. Mat. Sci.* **34** (1999) 3525.
12. J. M. HARRISON and J. F. NORTON, in "Behaviour of High Temperature Alloys in Aggressive Environments," edited by J. Kirman, J. B. Mariott, M. Merz, P. R. Sahm and D. P. Whittle (The Metals Society, London, 1980) p. 661.
13. H. M. TAWANCY and N. M. ABBAS, *J. Mat. Sci.* **27** (1992) 1061.
14. N. S. VANDAMME, B. H. WAYMAN and L. D. T. TOPOLESKI, *J. Mat. Sci.: Mater. in Med.* **14** (2003) 47.
15. ASM Committee on Gas Carburizing, "Gas Carburizing" (American Society for Metals, OH, 1964) p. 50.
16. T. A. RAMANARAYANAN and D. J. SROLOVITZ, *J. Electrochem. Soc* **132** (1985) 2268.
17. A. M. STAINES and T. BELL, *Thin Solid Films* **86** (1981) 201.
18. I. ASANO, T. ARAKI and Y. IKAWA, *Mater. Sci. Eng.* **A140** (1991) 461.
19. L. E. TOTH, "Transition Metal Carbide and Nitrides" (Academic Press, New York, 1971) p. 82.
20. T. EL-RAGHY and M. W. BARSOUM, *J. Appl. Phys.* **83** (1998) 112.
21. C. R. ANDERSON, private communication.

22. J. I. GOLDSTEIN, A. D. ROMIG, JR., D. E. NEWBURY, C. E. LYMAN, P. ECHLIN, C. FIORI, D. C. JOY and E. LIFSHIN, "Scanning Electron Microscopy and X-Ray Microanalysis" 2nd ed. (Plenum Press, New York, 1992) p. 526.

23. W. KÖSTER and F. SPERNER, *Arch. Eisenhüttenwesen* **26** (1955) 555.

Received 30 October 2003
and accepted 23 June 2004